High-Intensity Laser Induced Ion Acceleration from Heavy-Water Droplets

S. Karsch,[1,2] S. Düsterer,[3] H. Schwoerer,[3] F. Ewald,[3] D. Habs,[2] M. Hegelich,[1,2] G. Pretzler,[4] A. Pukhov,[4] K. Witte,[1] and R. Sauerbrey[3]

[1]*Max-Planck-Institut für Quantenoptik, 85748 Garching, Germany*
[2]*Universität München, 85748 Garching, Germany*
[3]*Friedrich-Schiller-Universität Jena, 07743 Jena, Germany*
[4]*Universität Düsseldorf, 40225 Düsseldorf, Germany*

(Received 29 August 2002; published 3 July 2003)

Fusion neutrons from a heavy water droplet target irradiated with laser pulses of 3×10^{19} W/cm^2 and from a deuterated secondary target are observed by a time-of-flight (TOF) neutron spectrometer. The observed TOF spectrum can be explained by fusion of deuterium ions simultaneously originating from two different sources: ion acceleration in the laser focus by ponderomotively induced charge separation and target-normal sheath acceleration off the target rear surface. The experimental findings agree well with 3D particle-in-cell simulations.

DOI: 10.1103/PhysRevLett.91.015001 PACS numbers: 52.38.Kd, 29.30.Hs, 52.65.Pp, 52.65.Rr

In recent years, high-intensity femtosecond (fs) lasers have been used to study the new area of relativistic laser-plasma interaction. In this context, one of the most dynamic topics is the acceleration of particles to very high energies over submillimeter distances [1–6]. Much research is directed towards the development of compact particle sources with a well characterized emission. Debris-free targets such as droplets are crucial for a reliable operation of those sources. However, the physics of laser particle acceleration is far from understood. In previous experiments, powerful ultrashort laser pulses were focused onto thin foil targets. Intense ion beams were detected behind the foil in laser direction. Two mechanisms of ion acceleration are presently under discussion. First, the ponderomotive charge separation at the front surface induces a double layer and the resulting static fields accelerate ions into the target [5,7,8]. Second, the laser-heated electrons propagate through the target, build up a space charge at the rear surface, and extract ions by the target-normal sheath acceleration (TNSA) mechanism [2,3,9–11]. The above experiments could clearly identify one of the two mechanisms to be dominant in their case. However, multidimensional particle-in-cell (PIC) simulations [9,12] suggest that in general both mechanisms work simultaneously and independently. With standard experimental techniques, it is hard to simultaneously quantify these two mechanisms, since predominantly protons are accelerated from oil or water contaminants present on both target surfaces.

In this work, for the first time heavy water droplets were irradiated at relativistic laser intensities. Deuterons causing fusion neutrons were used for separating the front and rear surface ion acceleration mechanisms. Deuterons are not naturally found in surface contaminants and are able to trigger fusion reactions such as $d(d, n)^3$He at low energies ($E_D \gtrsim 20$ keV), when using deuterated target material. The resulting fusion neutrons with their center-of-mass energy of 2.45 MeV can be used to obtain information on the incident deuteron energy and angular distribution [8,13–15] by measuring their kinematic shift. We use neutron time-of-flight (TOF) spectroscopy to get a clear distinction between front and rear surface accelerated deuterons and to determine the number and temperature of both species. Furthermore, the results are compared to PIC calculations.

The experiments (Fig. 1) were carried out at the Jena TW Ti:sapphire laser, delivering $\tau_L = 80$ fs, 10 Hz, $E = 600$ mJ pulses at $\lambda_L = 0.8$ μm. They were focused by an $f/2$ off-axis parabola to a spot size of 3 μm FWHM, leading to a focused intensity of $I_L = 3 \times 10^{19}$ W/cm^2 $= 30 \times I_{18}$. The target consisted of well defined 20 μm diameter D_2O droplets produced by a piezoelectrically modulated 10 μm diameter nozzle [16,17]. In spite of the difference in geometry from planar targets, the two acceleration mechanisms also work in droplets with some modifications discussed below. A secondary catcher target consisting of a 7 mm thick $(CD_2)_n$ disk (diameter 15 cm) was placed behind the

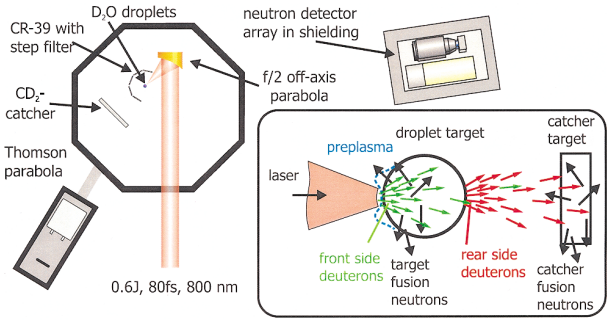

FIG. 1 (color). Experimental setup: Laser pulses are focused onto D_2O droplets. Deuterons from the laser focus create prompt fusion neutrons in the droplet, while deuterons from its back side cause delayed fusion reactions in the deuterated catcher target. A sketch of the two ion populations and the subsequent neutron production is shown in the inset.

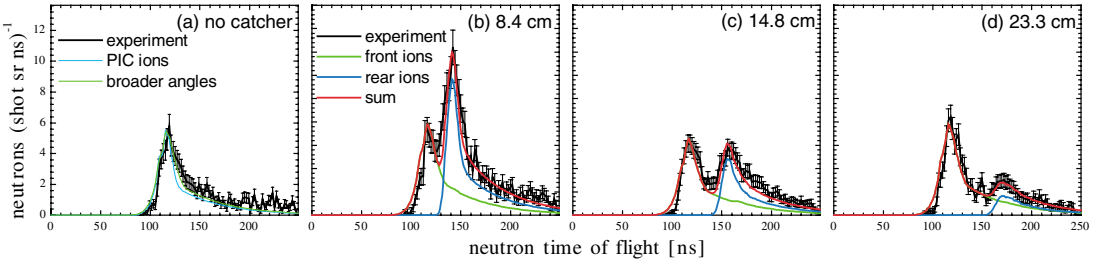

FIG. 2 (color). Neutron TOF spectra without a catcher (a) and with a catcher placed at different distances of (b) 8.4 cm, (c) 14.8 cm, and (d) 23.3 cm. The green and light-blue lines show simulations for ion emission of $T_{i,\mathrm{cold}} \sim 100$ keV and $T_{i,\mathrm{hot}} \sim 350$ keV from the front (see Fig. 3) for all cases, and blue corresponds to $T = 100$ keV (b),(c) or $T = 110$ keV (d) off the rear surface, respectively. The red line shows the sum spectrum.

droplet in laser direction (see Fig. 1) at distances of 8.4, 14.8, and 23.3 cm, covering 1.6, 0.7, and 0.3 sr, respectively. The fusion neutron TOF spectra were recorded by two NE110 plastic scintillation detectors. The time resolution of the whole system is ~1.5 ns and the detector efficiency is ~0.2. The detectors were placed at a distance of 240 cm from the focus at an angle of 143° to the laser axis inside a lead housing of 9 cm wall thickness to shield them against the gamma burst from the laser interaction. In order to suppress errors in the spectral shape from pileup, the count rate was kept low (~ 0.25 detected neutrons/shot). The presented spectra were recorded accumulating ~40 000 laser shots.

The neutron TOF spectra in Fig. 2 show the variation in spectral shape for different catcher distances. The spectrum in Fig. 2(a) was taken without the catcher and exhibits only a single peak from fusion neutrons created inside the droplet. With the catcher in place, a second peak appears in the spectrum [Figs. 2(b)–2(d)], indicating fusion in the catcher by deuterons accelerated from the droplet. When the catcher distance is enlarged, the second peak shifts to later times and gets broader. The distance between the two peaks corresponds to the ion TOF from the target to the catcher, whereas the broadening reflects the TOF dispersion of the ion spectrum. When the catcher was covered with a 200 μm thick undeuterated plastic foil, a spectrum similar to that shown in Fig. 2(a) was obtained for every catcher position, which rules out that the second peak might be due to neutrons created in the droplet and scattered by the catcher.

A Thomson parabola with a lower cutoff of 500 keV oriented at 15° to the laser axis measured deuterons with a maximum energy of ~1.2 MeV in a "hot tail" of 200–400 keV temperature and the onset of a strong colder component towards low energies. A qualitative analysis of the CR-39 detector sheets placed around the target showed an almost isotropic ion emission with broad, slight enhancements in the 0° (along laser axis) and 90° (perpendicular) directions. This combination of data from different detectors contains sufficient information for clearly separating the ion acceleration processes involved.

We first consider ion acceleration in the laser focus, similar to the results in [8,12,18]. It takes place at the interface between plasma and laser light, and its characteristics largely depend on geometry. The prepulse of the laser generates a plasma with a scale-length L_p estimated to 4–6 μm at the critical surface. The highly relativistic, tightly focused pulse bores a dip of depth $\approx \gamma L_p$ into the overdense preplasma ($\gamma = \sqrt{1 + I_{18}\lambda_L^2/2.74}$, λ_L in μm). The apex of the dip, however, is always located at the relativistic critical density ($n_r \approx \gamma n_c$, n_c: critical density), and therefore never reaches the bulk of the droplet. The deep dip expels most ions at large angles to the laser axis without respect to the target normal. This implies that the emission pattern is independent of the position of the focal spot on the droplet. This picture is experimentally confirmed by the 90° feature in the CR-39 data (for the 0° enhancement see further below) and by the timing of the first peak, which is a sensitive probe for the angle distribution of ions from the focus. Its measured position rules out a strong forward component (see below). References [8,18] describe similar cases; however, the laser parameters were quite different from ours. Their simulations were only 2D, thereby underestimating the depth of the formed dip and the predominant emission angle. Hence, we performed simulations with the 3D PIC code VLPL [19] to model the ions expelled from the focal volume. For both 0° and 45° (p-polarized) incidences, an 80 fs laser pulse of 4 μm diameter and an intensity of 3×10^{19} W/cm^2 enters the simulation box of $19 \times 16 \times 16$ μm^3. It contains a radially expanding preplasma of 4 μm scale length followed by a uniform bulk density of $16 n_c$. The most and fastest ions in both cases are emitted at large angles to the laser axis, as shown in Fig. 3(b). Figure 3(a) shows the ion spectra in different angle intervals to the laser axis. The angle-integrated ion spectrum contains ~10^{11} ions with a two-temperature exponential type spectrum ($T_{i,\mathrm{cold}} \sim 100$ keV and $T_{i,\mathrm{hot}} \sim 350$ keV). Since the most energetic ions are emitted at large angles, they cannot be seen in the Thomson parabola.

To simulate neutron TOF spectra from any given ion distribution, we developed the Monte Carlo neutron production code MCNEUT [20]. It tracks individual deuterons through the target, catcher, and detector geometry in 3D.

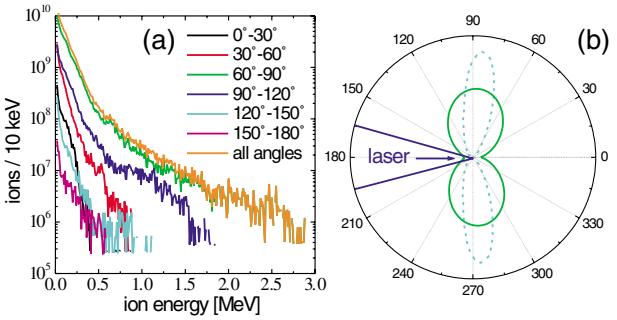

FIG. 3 (color). PIC results: (a) Ion spectra at different angle intervals to the laser axis and sum spectrum. (b) Angular distribution of the ions: from the PIC output (light-blue dotted line) and distribution modified for best match with the experiment (green solid line).

They are slowed down according to their energy loss in plasma (see below), while their fusion probability is determined from the DROSG2000 differential cross-section tables [21]. According to the resulting neutron energy, which is calculated from two-body reaction kinematics, the fusion probabilities are summed up in a TOF spectrum. Neutron scattering in the chamber and detectors was modeled by MCNP [22] neutron transport calculations and included in MCNEUT by a scattering function. Experimental laser pointing fluctuations which lead to different ion path lengths inside the droplet were modeled by moving the ion origin randomly across the droplet. When using the deuteron distribution from the PIC simulation as input, the computed neutron TOF spectrum is in good agreement with the experiment [see Fig. 2(a)]. An even better match is achieved with a broader angle distribution [see Fig. 3(b), green curve]. For a more forward-directed ion distribution the peak would shift to later times, which is not observed.

We now show that only a few front-side deuterons can penetrate the droplet, which contribute only weakly to the second peak. To calculate the number and spectrum of these transmitted ions, we must account for changes of the energy loss dE/dx in the droplet that gets ionized by fast electrons. In plasma, dE/dx is enhanced for fast ions, $v_i > v_{\mathrm{th}}$, and strongly reduced for slow ions, $v_i < v_{\mathrm{th}}$, where v_i is the ion velocity and v_{th} is the thermal electron velocity. We assumed that 20% of the laser energy is converted into fast electrons ($T_{\mathrm{hot}} = 1.47$ MeV given by the ponderomotive scaling [23]), which are emitted in a $\pm 40°$ FWHM plume around the laser axis. They lose their energy by collisional stopping. The local temperature can then be determined from SESAME equation-of-state tables [24]. The effective charge state is estimated from a Thomas-Fermi model [25]. These values are put into our stopping model, which treats the contribution of bound target electrons by the SRIM tables [26] and that of free electrons by a low-energy extension of the plasma energy loss from [27]. With these modifications to MCNEUT, we calculated the neutron spectra using only *front-side* ions. Their angle distribution was assumed isotropic to overestimate the second peak compared to the distribution in Fig. 3(b). The penetrating ions cause only a small second peak (Fig. 4). The overall effect of target heating on the neutron spectra is small ($\sim 10\%$ change in neutron yield; compare red and black curves in Fig. 4).

This calculation shows that the second peak in the measured TOF spectra *cannot* be explained by front-side ions alone. Therefore, a second deuteron population is postulated that does not interact in the droplet and is therefore accelerated off the droplet rear surface. It can be explained by the TNSA [2,9] mechanism: hot electrons from the laser focus penetrate the target and exit at the rear side. They are bound to the target by building up a space charge that forms a sheath extending approximately one Debye length, $\lambda_D = (\epsilon_0 k T_{\mathrm{hot}}/e^2 n_{e,\mathrm{hot}})^{1/2}$, into vacuum. Thereby a strong field is set up at the rear surface, $E_{\mathrm{stat}} \approx k T_{\mathrm{hot}}/e\lambda_D \sim 1$ TV/m [2]. Here, $n_{e,\mathrm{hot}}$ is the density of hot electrons at the target rear surface. The initial lateral spread of this electron sheath depends on the divergence and the transport of the electron beam through the target. Since the droplet is isolated from the environment, the electrons cannot escape and the sheath later spreads around the surface to form an almost uniform halo. The TNSA mechanism—in planar foils responsible for the ion acceleration normal to the rear side—therefore accelerates ions into 4π with only a slight enhancement in 0° (due to the initial sheath at the rear side) in our case, which explains the CR-39 findings. Assuming ion acceleration into 4π, we can put model spectra of TNSA ions into MCNEUT to calculate the TOF spectra of fusion neutrons from the catcher target. The good agreement of the simulation of the second neutron peak with the measurement is shown in Fig. 2. Comparing the dependence of the measured shift of the position of the second peak with the catcher distance to that calculated, we can determine the ion temperature (Fig. 5). The experimental values agree well with a temperature of the rear-side ions of 100 ± 30 keV. This is quite low compared to other experiments, but can be explained by our laser parameters and specific geometry.

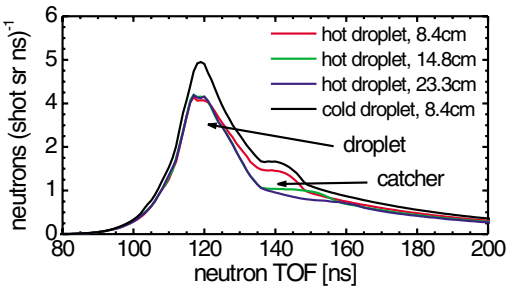

FIG. 4 (color). Simulated neutron spectra, assuming only front-accelerated deuterons (isotropic distribution, enhancing the second peak), for different catcher distances. The stopping is treated for a cold and an electron-heated (hot) droplet.

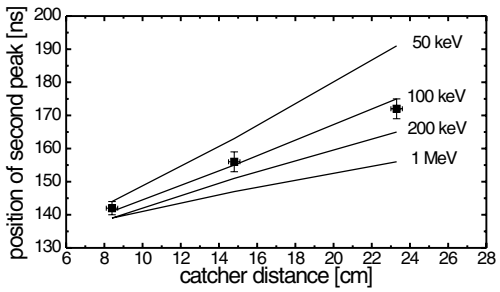

FIG. 5. Position of the second peak for different ion temperatures as predicted by MCNEUT and experimental data.

Mackinnon *et al.* [28] report that in a 2D PIC simulation for 20 μm thick planar targets and 100 fs, 10 J, 1×10^{20} W/cm^2 laser pulses the expansion velocity of the rear surface was 0.05c, corresponding to $T_i = 1.15$ MeV. Assuming the same pulse duration and conversion efficiency η of laser energy W into electrons for our experiment and [28], the hot electron density scales as $n_{e,\mathrm{hot}} \propto \eta W/(kT_{\mathrm{hot}} A \lambda_D)$, A being the area of the sheath. The accelerating field then scales as $E_{\mathrm{stat}} \propto e\eta W/(\epsilon_0 kT_{\mathrm{hot}} A)$. At $\pm 40°$ divergence, at JanUSP the electron beam exits the target in a circle of radius $\sim\sqrt{3} r_t$; $A = 3\pi r_t^2$ (r_t = target thickness/2 = droplet radius), whereas in our case the electrons spread around the whole droplet ($A = 4\pi r_t^2$). With the energy and intensity in the two cases, we estimate a 10× lower static field in our case. Since τ_L is about equal in both cases, a mean ion energy of 115 keV is obtained in good agreement with our observation.

By varying the ion number, we can find the best match to the experimental peak height. The result is shown in Figs. 2(b)–2(d) together with the measurements. For a best-fit temperature of ~100 keV, the second peaks in the three runs were caused by 4.8×10^{10} (8.4 cm distance), 2×10^{10} (14.8 cm), and 9×10^9 (23.3 cm) ions hitting the catcher. Taking into account the catcher solid angles at different distances, this corresponds to a total number of surface accelerated ions of 3.8×10^{11}, 4.5×10^{11}, and 4.2×10^{11}, respectively. Since these numbers are in good mutual agreement, the assumption of isotropic ion acceleration fits our neutron data. The total number of these ions, as inferred from the area of the second peak, is 10× higher than that needed to explain the first peak, ruling out that the small fraction of transmitted front-side ions significantly contribute to the second peak.

In conclusion, we report a new plasma-diagnostics application of deuterium ions accelerated by a tabletop 10 Hz multiterawatt laser. For the first time, relativistic interactions with droplets were studied, and the use of deuterated primary and secondary targets and fusion neutron spectroscopy made it possible to distinguish between ions accelerated from both target surfaces in a single experiment. Our findings are consistent with two different acceleration mechanisms, namely, acceleration in the laser focus by ponderomotive charge-separation fields and acceleration off the droplet surface by the TNSA mechanism. The measurements supported by simulations show that both acceleration processes work independently at the same time. Under our conditions many more ions are emitted from the rear surface than from the front, albeit at lower energies. Although the absolute ion temperatures are rather low, the conversion of laser energy to ion energy is substantial: We arrive at a mean energy content of ~1 mJ for the front-side ions and ~6 mJ for the surface accelerated ions, leading to a total conversion efficiency of about 1%.

We thank H. Ruhl, Y. Sentoku, P. Audebert, S. Gordienko, and T. Cowan for fruitful discussions, W. Guenther for analyzing the CR-39 detectors and the Jena laser team. This work was supported by the DFG, Projects No. HA 1101/7-2 and No. SCHW 766/2-2, and EURATOM-IPP.

[1] D. Gordon *et al.*, Phys. Rev. Lett. **80**, 2133 (1998).
[2] S. Hatchett *et al.*, Phys. Plasmas **7**, 2076 (2000).
[3] M. Hegelich *et al.*, Phys. Rev. Lett. **89**, 085002 (2002).
[4] C. Gahn *et al.*, Phys. Rev. Lett. **83**, 4772 (1999).
[5] A. Maksimchuk *et al.*, Phys. Rev. Lett. **84**, 4108 (2000).
[6] H. Schwoerer *et al.*, Phys. Rev. Lett. **86**, 2317 (2001).
[7] E. Clark *et al.*, Phys. Rev. Lett. **84**, 670 (2000).
[8] N. Izumi *et al.*, Phys. Rev. E **65**, 036413 (2002).
[9] S. Wilks *et al.*, Phys. Plasmas **8**, 542 (2001).
[10] R. Snavely *et al.*, Phys. Rev. Lett. **85**, 2945 (2000).
[11] A. MacKinnon *et al.*, Phys. Rev. Lett. **86**, 1769 (2001).
[12] A. Pukhov, Phys. Rev. Lett. **86**, 3562 (2001).
[13] D. Hilscher *et al.*, Phys. Rev. E **64**, 016414 (2001).
[14] L. Disdier *et al.*, Phys. Rev. Lett. **82**, 1454 (1999).
[15] S. Karsch *et al.*, Laser Part. Beams **17**, 565 (1999).
[16] S. Düsterer *et al.*, Appl. Phys. B **73**, 693 (2001).
[17] L. Rymell *et al.*, Opt. Commun. **103**, 105 (1993).
[18] C. Toupin *et al.*, Phys. Plasmas **8**, 1011 (2001).
[19] A. Pukhov *et al.*, Phys. Plasmas **5**, 1880 (1998).
[20] S. Karsch, MPQ Report No. 279, 2003.
[21] M. Drosg, DROSG2000 (www.iaea.org, 2000).
[22] J. Briesmeister *et al.*, Los Alamos Report No. LA-12625-M, 1997.
[23] S. Wilks *et al.*, Phys. Rev. Lett. **69**, 1383 (1992).
[24] S. Lyon *et al.*, Los Alamos Report No. LA-UR-3407, 1992 (unpublished).
[25] R. More, in *Handbook of Plasma Physics* (North-Holland, Amsterdam, 1991).
[26] J. Ziegler *et al.*, SRIM 2000 (www.srim.org, 2000).
[27] J. Jackson, *Classical Electrodynamics* (Wiley, New York, 1975).
[28] A. Mackinnon *et al.*, Phys. Rev. Lett. **88**, 215006 (2002).